Computationally designed peptide macrocycle inhibitors of New Delhi metallo-β-lactamase 1

Vikram Khipple Mulligan[a,b,1], Sean Workman[c,2], Tianjun Sun[c,2], Stephen Rettie[b], Xinting Li[b], Liam J. Worrall[c], Timothy W. Craven[b], Dustin T. King[c], Parisa Hosseinzadeh[b], Andrew M. Watkins[d], P. Douglas Renfrew[a], Sharon Guffy[e], Jason W. Labonte[f,g], Rocco Moretti[h], Richard Bonneau[a,i,j], Natalie C. J. Strynadka[c], and David Baker[b]

[a]Center for Computational Biology, Flatiron Institute, New York, NY 10010; [b]Institute for Protein Design, Department of Biochemistry, Molecular Engineering and Sciences, University of Washington, Seattle, WA 98195; [c]Department of Biochemistry and Molecular Biology and the Centre for Blood Research, University of British Columbia, Life Sciences Centre, Vancouver, BC V6T 1Z3, Canada; [d]Department of Biochemistry, Stanford University School of Medicine, Stanford, CA 94305; [e]Department of Biochemistry and Biophysics, University of North Carolina, Chapel Hill, NC 27599; [f]Department of Chemistry, Franklin & Marshall College, Lancaster, PA 17604; [g]Department of Chemical & Biomolecular Engineering, Johns Hopkins University, Baltimore, MD 21218; [h]Center for Structural Biology, Department of Chemistry, Vanderbilt University, Nashville, TN 37240; [i]Center for Genomics and Systems Biology, Department of Biology, New York University, New York, NY 10003; and [j]Courant Institute of Mathematical Sciences, Department of Computer Science, New York University, New York, NY 10012

Edited by Susan Marqusee, University of California, Berkeley, CA, and approved February 10, 2021 (received for review June 19, 2020)

The rise of antibiotic resistance calls for new therapeutics targeting resistance factors such as the New Delhi metallo-β-lactamase 1 (NDM-1), a bacterial enzyme that degrades β-lactam antibiotics. We present structure-guided computational methods for designing peptide macrocycles built from mixtures of L- and D-amino acids that are able to bind to and inhibit targets of therapeutic interest. Our methods explicitly consider the propensity of a peptide to favor a binding-competent conformation, which we found to predict rank order of experimentally observed IC_{50} values across seven designed NDM-1- inhibiting peptides. We were able to determine X-ray crystal structures of three of the designed inhibitors in complex with NDM-1, and in all three the conformation of the peptide is very close to the computationally designed model. In two of the three structures, the binding mode with NDM-1 is also very similar to the design model, while in the third, we observed an alternative binding mode likely arising from internal symmetry in the shape of the design combined with flexibility of the target. Although challenges remain in robustly predicting target backbone changes, binding mode, and the effects of mutations on binding affinity, our methods for designing ordered, binding-competent macrocycles should have broad applicability to a wide range of therapeutic targets.

antibiotic resistance | drug design | protein folding | peptide macrocycles | computational design

Despite the impact of vaccination and antibiotics, emerging pathogens remain a major threat to public health. In particular, the rise of bacteria resistant to β-lactam antibiotics threatens the clinical utility of one of the primary classes of antibacterial drugs (1). Resistance also hinders the clinical management of sepsis, currently the most common cause of death in hospitals, and is a major concern for treating bacterial infection more generally (1, 2). Mechanisms of resistance are diverse, but many resistant pathogens employ β-lactamase enzymes that are able to degrade β-lactam antibiotics (3). The New Delhi metallo-β-lactamase 1 (NDM-1) was identified in Sweden in 2008 and in many other countries around the world shortly thereafter (4–6). This enzyme can degrade even β-lactams of last resort, such as the carbapenems (4, 7). As we enter an era in which even the most chemically diverse β-lactam antibiotics are susceptible to degradation by pathogen lactamases with broad substrate specificities, the prospects for developing new, degradation-resistant chemical variants of these antibiotics grow fainter. This makes the strategy of combating resistance mechanisms with an inhibitor coadministered with an existing β-lactam antibiotic more attractive. However, there is no drug that is currently clinically approved to inhibit NDM-1 or any other metallo-β-lactamase (8).

The current drug discovery process has shown exponentially decaying efficiency over the past several decades in terms of new drugs found per research dollar invested (9). Many factors contribute to this inefficiency, including the large numbers of lead compounds that show poor pharmacokinetic, pharmacodynamic, or toxicological properties in late-stage animal or clinical studies. A key early-stage bottleneck is the process of screening hundreds of thousands of candidate molecules in order to identify an initial hit. Rational structure-based drug design methods, which propose a small pool of candidate molecules for experimental screening that is likely to be enriched for hits, represent an attractive alternative to undirected screening-based approaches to address this bottleneck. Since these methods allow larger pools of initial hits to be identified at lower experimental cost, they

Significance

Peptide macrocycles are a promising class of drugs, but their weakness is conformational flexibility: target affinity can be limited by an unfavorable transition from a disordered unbound state to an ordered bound state. We introduce general computational methods for stabilizing peptide macrocycles in binding-competent conformations as part of the process of designing for binding to a target protein. As a proof of principle, we apply our methods to create inhibitors of the New Delhi metallo-β-lactamase 1, an antibiotic resistance factor. Predictions of peptide rigidity correlate with experimental success, allowing designs to be prioritized for synthesis and testing. These methods should contribute to the design of peptide macrocycle inhibitors of diverse targets of therapeutic interest.

Author contributions: V.K.M., D.T.K., N.C.J.S., and D.B. designed research; V.K.M., S.W., T.S., S.R., X.L., L.J.W., and D.T.K. performed research; V.K.M., T.W.C., P.H., A.M.W., P.D.R., S.G., J.W.L., R.M., and R.B. contributed new reagents/analytic tools; V.K.M., S.W., T.S., S.R., X.L., and L.J.W. analyzed data; and V.K.M. and D.B. wrote the paper.

Competing interest statement: Rosetta software has been licensed to numerous not-for-profit and for-profit organizations. Rosetta Licensing is managed by UW CoMotion, and royalty proceeds are managed by the RosettaCommons. Under institutional participation agreements between the University of Washington, acting on behalf of the RosettaCommons, their respective institutions may be entitled to a portion of revenue received on licensing Rosetta software including programs described here. R.B. and D.B. are unpaid board members of RosettaCommons. V.K.M. is a co-founder of Menten AI, in which he holds equity.

This article is a PNAS Direct Submission.

[1]To whom correspondence may be addressed. Email: vmulligan@flatironinstitute.org.

[2]S.W. and T.S. contributed equally to this work.

This article contains supporting information online at https://www.pnas.org/lookup/suppl/doi:10.1073/pnas.2012800118/-/DCSupplemental.

Published March 15, 2021.

could also help to ease later-stage bottlenecks by providing more choice for lead identification and optimization, permitting candidates with higher probabilities of late-stage success to be carried forward.

High-affinity binding of a drug to its target depends on having a large free-energy gap between the bound and unbound states: the enthalpic favorability of the interactions between drug and target must outweigh the entropic cost of binding. Design methods generally focus on maximizing favorable interactions between a designed molecule and a target protein to maximize affinity and specificity. Unfortunately, as such methods append chemical groups to increase interactions with the target, the designed molecule becomes more flexible. This creates a mounting entropic cost associated with ordering the molecule so that it can bind, which reduces affinity and also introduces the possibility that the molecule may adopt alternative conformations that permit off-target interactions, which would hinder specificity (10). An ideal design method would maximize the favorability of intermolecular interactions between a drug and its target while simultaneously maximizing the rigidity of the drug in the unbound state, since both factors are critical for binding.

We previously reported computational methods, implemented within the Rosetta software suite (11), for designing and validating rigidly structured peptide macrocycles built from mixtures of natural and nonnatural amino acids (12–14). Rigidly structured peptide macrocycles should lose less conformational entropy on binding, and our working hypothesis is that this can address the problems hindering flexible meso-scale molecules and enable higher-affinity binding. Peptide macrocycles also combine many of the attractive properties of large-molecule (protein) therapeutics and of small-molecule drugs (15). Like protein therapeutics, peptide macrocycles present large surface areas for high-affinity, specific recognition of targets. This shared property of meso-scale and large-molecule therapeutics could account for their higher observed success rates when they reach clinical phases of testing (16). At the same time, macrocyclization and incorporation of D-amino acids reduce recognition by the immune system and sensitivity to proteases, both of which are factors limiting the use of cellularly produced proteins as drugs (13, 17). Like small molecules, peptide macrocycles can be produced in large molar quantities, stored robustly, and administered relatively easily. Some natural peptide macrocycles, such as cyclosporine A, show oral bioavailability and cell permeability comparable to small-molecule drugs (18).

Starting with the X-ray crystal structure of NDM-1 bound to L-captopril, a weak small-molecule inhibitor of NDM-1 (19–21), we adapted our peptide macrocycle design methods to create inhibitors of NDM-1 that are simultaneously optimized for favorable interactions with the target and for rigidity in the binding-competent conformation. We promoted the latter by designing favorable internal interactions in this conformation and by strategic incorporation of rigidifying building blocks to render alternative conformations less favorable. Through enzyme inhibition assays and crystallographic studies, we show that our top design inhibits NDM-1 with 50-fold greater potency than the D-captopril control while binding to the active site in the designed binding mode and adopting the designed binding conformation. Unlike conventional drug screening approaches involving enormous compound libraries, our methods allowed us to shift most of the high-throughput exploration to in silico stages of the pipeline and to find hits from an initial experimental screen of only seven peptides. The computational methods developed here represent a general means of designing rigidly structured peptide macrocycles to bind to proteins of therapeutic interest, applicable to many targets beyond NDM-1.

Results and Discussion

Rationale and Approach for Structure-Guided Design. NDM-1 is competitively inhibited by both L- and D-isoforms of captopril. Although the D-isoform is reported to be a 25-fold more potent inhibitor (21), only the L-isoform had an available X-ray crystal structure (Protein Data Bank [PDB] ID 4EXS) that we could use as a starting point when we began our peptide design work (Fig. 1*A*) (20). L-captopril occludes the NDM-1 active site cleft. Adjacent to this cleft are an ordered front loop (FL) consisting of amino acids 210 through 228 and a flexible hinge loop (HL) consisting of amino acids 64 through 73. The HL shows considerable conformational heterogeneity from one crystal structure to another or even in copies of the molecule in the asymmetric unit of a single crystal structure (Fig. 1*B*). The HL flexibility presents a major challenge for the design of larger inhibitors able to make more molecular contacts. For purposes of computational peptide design, we supposed that the observed HL conformations in available crystal structures represent relatively low-energy conformations of this loop. Since the conformation in chain B of PDB structure 4EXS presents Phe70 in a position likely to permit favorable hydrophobic interactions with an inhibitor, we chose this conformation for our in silico design work.

L-captopril resembles a D-cysteine-L-proline dipeptide with a methyl group replacing the terminal amine. When it binds to the NDM-1 active site, the sulfur atom intercalates between and binds to the two catalytic zinc atoms, and the proline fills the space of the active site cleft (Fig. 1*C*). In silico, we converted the L-captopril methyl group in the 4EXS structure to an amine, yielding a D-cysteine-L-proline dipeptide "stub" bound in the NDM-1 active site. We then extended this stub, prepending a three-residue polyglycine chain by an amide bond to the D-cysteine, and similarly appending a three-residue polyglycine chain to the C terminus of the L-proline to yield an eight-residue peptide (Fig. 1*D*). Using the Rosetta generalized kinematic closure method (12, 13), we sampled conformations of this chain that were compatible with an amide bond linking the two termini and with favorable intramolecular backbone hydrogen bonding, keeping the D-cysteine-L-proline starting stub fixed.

For each conformation sampled, we designed sequences to maximize favorable interactions with the target while favoring the designed conformation (see below) using Rosetta side-chain packing methods, sampling L- and D-amino acids at positions able to accommodate each respectively (Fig. 1*E*). This was followed by a Monte Carlo-based refinement procedure in which we sampled small perturbations of the peptide conformation using generalized kinematic closure, reoptimizing side-chain identities and rotamers for each conformation sampled. We filtered this initial pool of several hundred designs based on the number of internal hydrogen bonds, shape complementarity to the target, and atomic clashes (*Materials and Methods*). To assess diversity of backbone conformations in the filtered population, we assigned each amino acid residue to one of four conformational bins, designated A, B, X, and Y, and representing left-handed α-helical, left-handed β-strand, right-handed α-helical, and right-handed β-strand conformations, respectively; these are described in greater detail in *SI Appendix*, section 2.1.6. We selected peptides with diverse backbone bin strings, and since we hypothesized that rigidity would be a key determinant of success, these were subjected to in silico conformational landscape analysis using the Rosetta simple_cycpep_predict protocol (12, 13) to identify designs predicted to fold to the binding-competent conformation in the absence of the target. We used the P_{Near} metric described previously (12, 13, 15), which approximates the fractional occupancy (Boltzmann weight) of the designed conformation amid large sets of alternative conformations generated by extensive conformational sampling. P_{Near} values close to 0 indicate little predicted propensity to favor the

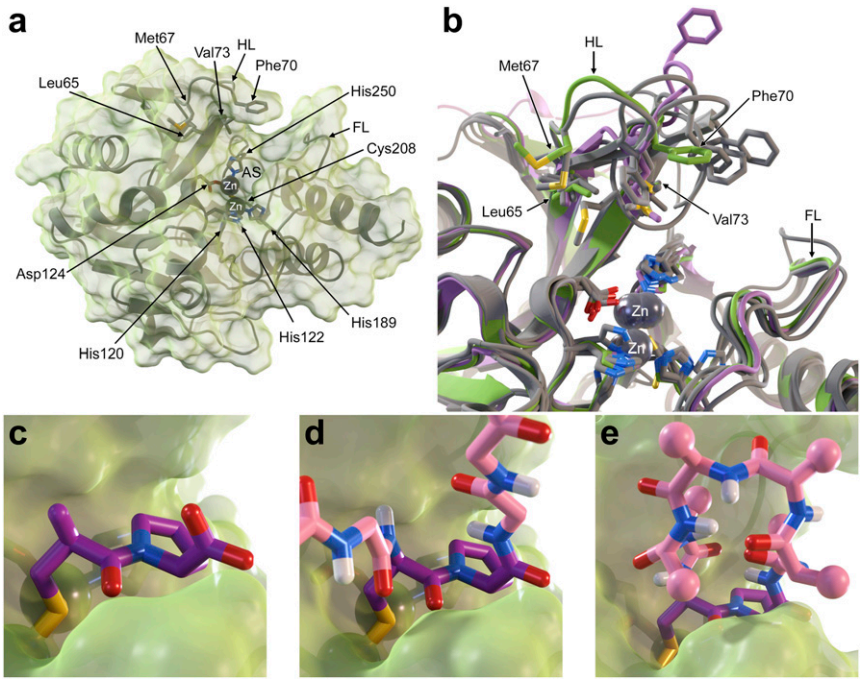

Fig. 1. Computational design approach for generating peptide macrocycle inhibitors of NDM-1. (*A*) Structure of NDM-1 (PDB ID 4EXS), chain B. The active site binds catalytic zinc atoms and is flanked by an ordered FL and a flexible HL. Hydrophobic amino acid residues on the inner face of the HL, and metal-coordinating residues, are labeled. (*B*) Comparison of a subset of NDM-1 crystal structures. PDB IDs 3RKJ, 3S0Z, 3ZR9, and 4HL1 are shown in gray. In lavender and green are PDB ID 4EXS, chains A and B, respectively. Where most of the structure, including the FL, is rigid, the HL shows extensive conformational flexibility, putting inner-face hydrophobic side chains (labeled) in diverse positions. (*C*) Crystal structure of NDM-1 active site (green) with L-captopril (purple) bound (PDB ID 4EXS, chain B). Active-site zinc atoms are shown beneath the surface as spheres. (*D*) In silico conversion of L-captopril to a D-proline, L-cysteine dipeptide (purple) flanked by polyglycine sequences (pink). (*E*) Rapid in silico sampling of closed conformations of a peptide macrocycle containing the D-cysteine, L-proline stub (purple), and flanking sequences (pink) in the context of the NDM-1 active site, using the generalized kinematic closure approach. For each closed conformation, Rosetta design heuristics were used to find side-chain identities and conformations (represented here by spheres).

binding-competent conformation, while values close to 1 indicate high predicted propensity for the binding-competent conformation (*SI Appendix*, section 1.5.4).

Inhibitory Activity of Designed Peptides. We chose seven designs for synthesis and experimental characterization, designated NDM1i-1A through NDM1i-1G, as shown in Fig. 2. These designs were selected for having favorable Rosetta peptide-target interaction energies, possessing diverse backbone conformations and intramolecular hydrogen bond patterns, and presenting hydrophobic side chains to interact with Leu65, Met67, Phe70, and Val73 on the inner hydrophobic face of the NDM-1 HL. The selected peptides were all optimized primarily for favorable interactions with the target during the design process, with folding propensity promoted by favoring conformationally constrained D- and L-proline residues. As such, they had P_{Near} values that ranged from 0.64 (NDM1i-1C) to 0.96 (NDM1i-1G).

We synthesized and purified the seven peptides and carried out NDM-1 inhibition assays using 1.5 μM nitrocefin as the substrate (Fig. 2, column *v*) at different designed inhibitor concentrations. IC_{50} values were estimated as described in *SI Appendix*, section 3.3. As a positive control, we used the D-captopril isoform (a more potent inhibitor than the L-captopril starting point for design), which had an IC_{50} value of 59.7 ± 6.3 μM (*SI Appendix*, Fig. S1). High-quality fits to the data for all peptides and controls were consistent with the expected 1:1 stoichiometry of binding (see *SI Appendix*, section 3.3 for details). All of the peptides but NDM1i-1C had IC_{50} values lower than D-captopril, with the top peptide, NDM1i-1G, having an IC_{50} value of 1.2 ± 0.1 μM, more than 50 times more potent than D-captopril.

Since a robust peptide therapeutic design pipeline would benefit considerably from computational metrics that could reliably rank designs to prioritize syntheses and experiments, we next examined which metrics best correlated with experimental success across our initial batch of designs. As noted above, the free energy of binding of a flexible molecule to a fixed target can be decomposed as the sum of two terms: $\Delta G_{binding}$, the interaction free energy between the molecule and the target in the bound complex, and $\Delta G_{folding}$, the free energy of ordering the flexible molecule into the conformation adopted in the complex. Rosetta estimates of $\Delta G_{binding}$ using the difference in energy between the bound and unbound conformations (with limited conformational sampling of side chains across replicates) had little correlation with observed IC_{50} values (Fig. 3*A*). Since $\Delta G_{folding} = -RTln(K_{eq}) = -RTln\left(\frac{f}{1-f}\right)$, where f is the fractional occupancy of the folded state at equilibrium, we can estimate folding free-energy changes using the P_{Near} metric described above as the approximate value of f (*SI Appendix*, section 1.5.4). Such estimates of $\Delta G_{folding}$, which are based on near-exhaustive sampling of the conformations of the peptide macrocycle in isolation, converge robustly and correlate well with the logarithm of the IC_{50} value—so well that the rank order of computed $\Delta G_{folding}$ values matches the rank order of experimental IC_{50} values (Fig. 3*B*). Comparisons to conformational sampling simulations using earlier versions of the Rosetta energy function reveal that improvements to the energy function accuracy using small-molecule fluid simulations for parameter tuning (22, 23) have improved the correlation between estimated $\Delta G_{folding}$ and observed IC_{50} (*SI Appendix*, Fig. S2). There are several possible explanations for the lack of correlation between our $\Delta G_{binding}$ estimates and the observed IC_{50} values. First, the differences in the interaction energies across these seven designs are likely to

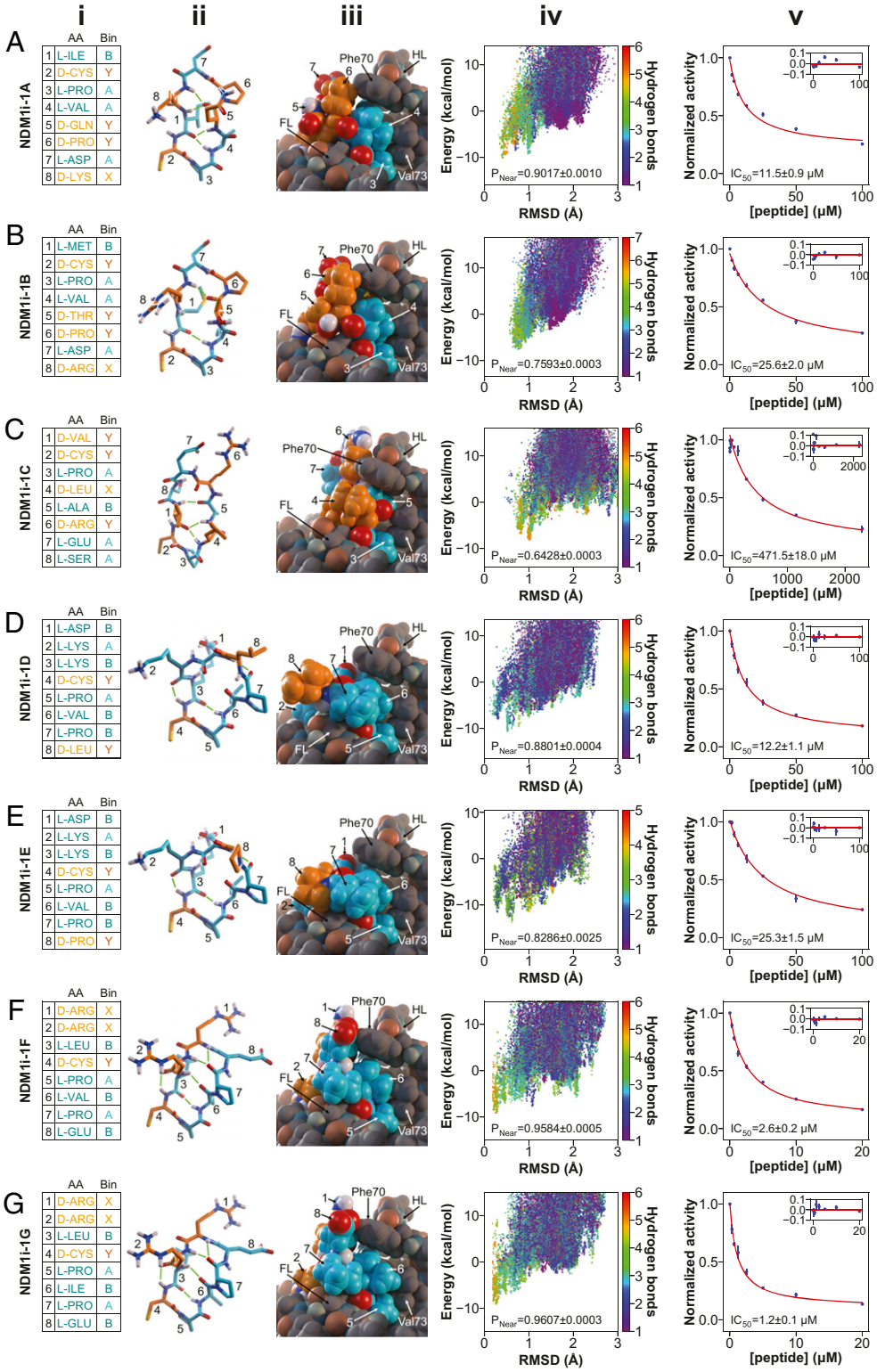

Fig. 2. Designed eight-residue peptide macrocycle inhibitors of NDM-1, designated NDM1i-1A (*A*) through NDM1i-1G (*G*). (*i*) Amino acid sequences (AA) and backbone conformational bins (Bin) of designed peptides. In this and the following two columns, L-amino acids are shown in cyan and D-amino acids in orange. Backbone conformational bins are described in *SI Appendix*, section 2.1.6. (*ii*) Peptide design computer models shown as stick representations. Intramolecular backbone hydrogen bonds are shown as green lines. Sequence numbering is as shown in *i*. (*iii*) Space-filling computer models of designed peptides in the NDM-1 active site, with NDM-1 shown in gray. The HL, FL, and interacting residues Phe70 and Val73 are indicated. (*iv*) Conformational landscape analysis performed with the Rosetta simple_cycpep_predict application, showing computed energy of the peptide modeled in isolation plotted against rmsd to its designed binding conformation. Each point represents a separate conformational sampling attempt. Colors indicate the number of intramolecular backbone hydrogen bonds observed in the sampled conformation. P_{Near} values are indicated, with the mean and SE of three independent large-scale conformational sampling simulation replicates reported. (*v*) Experimentally measured activity of NDM-1 (vertical axis) in the presence of varying concentrations of peptide (horizontal axis). Points are mean of three independent replicates, and error bars represent the SEM. Red curves show fits to the Hill equation, with IC_{50} values and fit confidence indicated on each plot. (*Insets*) Fit residuals.

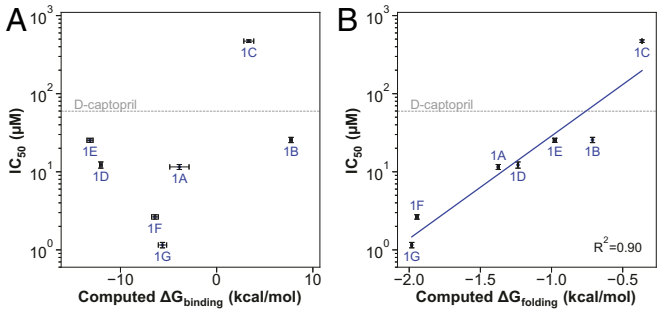

Fig. 3. Comparison of computationally predicted metrics and experimentally measured IC_{50} values for peptides NDM1i-1A through NDM1i-1G. The IC_{50} value for D-captopril is shown as dashed gray lines. (*A*) Comparison of experimentally measured IC_{50} values (vertical axis) with Rosetta-computed estimates of $\Delta G_{binding}$ (horizontal axis). Vertical error bars represent uncertainty in fitted parameters, and horizontal error bars represent SEM of 20 replicates of the computation, with optimization of side-chain conformations in bound and unbound states producing some variation from replicate to replicate. No correlation is observed. (*B*) Comparison between experimentally measured IC_{50} values and estimates of $\Delta G_{folding}$ ($-RT\ ln(P_{Near}/(1-P_{Near}))$ as described in the *SI Appendix*) obtained from computed energy landscapes (for examples, see Fig. 2, column *iv*). Vertical error bars are as in *A*. Horizontal error bars represent the SEM of three independent landscape simulations. The blue line shows the empirical line of best fit with R^2 value indicated.

be small since all designs tested were extensively optimized during the design process to maximize favorable interactions with the target. Second, the Rosetta interaction energy is an imperfect estimate of the actual binding free energy: entropic costs of ordering the side chains and backbone of the target (which can be substantial given the flexibility of the loops) are neglected, and the Rosetta force field, like any molecular force field, involves numerous approximations.

The correlation between computed $\Delta G_{folding}$ and observed IC_{50} supports our working hypothesis that rigidity in a binding-competent conformation is a key determinant of high-affinity binding when designing these meso-scale molecules: a favorable $\Delta G_{folding}$ is clearly necessary (but not sufficient, since favorable interactions are also needed) for high-affinity binding. Completed designs can be evaluated using extensive energy landscape calculations, as we describe with our P_{Near} metric, which estimates the probability that the design adopts the target conformation (instead of the myriad other possible conformations). But how can $\Delta G_{folding}$ be optimized during design? We were able to achieve this by implicit negative design (24), incorporating design-centric scoring terms that promote sequences favoring the designed target conformation over other possible conformations (*SI Appendix*, section 1.3). These included an amino acid composition ("aa_composition") term, which we used to penalize fewer than three D- or L-proline residues to discourage many alternative conformations in designs, and an "hbnet" term, favoring designs with internal hydrogen bond networks, which are unlikely to be compatible with most alternative conformations. In any given design challenge, the weights and parameters of these terms can be adjusted to determine the combination that best guides sequence design trajectories to those sequences most favoring the target-binding conformation.

Inhibitory Activity of Variants of NDM1i-1G. We next carried out in silico mutagenesis of the top inhibitor NDM1i-1G, examining the effect on P_{Near} of mutations at every position to each of 46 possible amino acid types. As shown in *SI Appendix*, Fig. S3, the peptide is highly mutable, with many chirality-preserving mutations, as well as some chirality-inverting mutations, preserving the fold propensity. We synthesized four point mutants that were predicted to preserve the fold and to interact favorably with the target: D-Arg1→D-Thr (r1t), L-Leu3→L-Tyr (L3Y), L-Ile6→L-Leu (I6L), and L-Glu8→2-aminoisobutyric acid (E8AIB), along with seven combinations of these mutations (*SI Appendix*, Figs. S4 and S5). These peptides are designated NDM1i-2A through 2K. Several of these mutations increased IC_{50} values without reducing computed $\Delta G_{folding}$ values (*SI Appendix*, Fig. S6), suggesting that the manual introduction of these mutations to an optimized design weakened interactions with the target. A triple mutation with an IC_{50} value of 1.8 ± 0.1 μM (NDM1i-2J, bearing mutations L3Y/I6L/E8AIB) showed greater inhibition than any of the individual mutations or the L3Y/I6L double mutation (NDM1i-2H). The IC_{50} value was close to that of the NDM1i-1G (1.2 ± 0.1 μM) starting point, suggesting that there are multiple opportunities for finding variant inhibitors in the local sequence space of these peptides. These experiments are described in greater detail in *SI Appendix*, section 4.2.

Crystal Structures of Inhibitory Peptides Bound to NDM-1. To gain greater insight into the inhibition of NDM-1 by some of the top inhibitors, we crystallized the enzyme and solved structures by X-ray crystallography in complex with peptides NDM1i-1F and NDM1i-1G. Fig. 4 shows a comparison of the design and crystal structure of NDM1i-1G bound to NDM1. The binding mode observed in the crystal structure closely resembles that in the design, with the D-Cys-L-Pro stub coordinating active-site zinc residues as the L-captopril starting compound does. Peptide residues L-Leu3 and L-Ile6 pack against NDM-1 HL residues Met67 and Phe70, albeit with slightly different packing interactions than designed. This is due to flexibility of the HL, which moves in the crystal structure relative to the design structure (HL backbone heavyatom rmsd 3.1 Å), causing the peptide to rotate slightly about the stub residues in the opposite direction (peptide backbone heavyatom rmsd 1.8 Å) (Fig. 4*C*). Despite this, the internal conformation of the peptide remains rigid: when the peptide portion of the design model is aligned with the peptide portion of the crystal structure, the rmsd is 0.3 Å (Fig. 4*D*). Designed ionic interactions between NDM1i-1G residue D-Arg2 and NDM-1 residues Glu152 and Asp223 were blocked by the binding of a zinc ion to the anionic NDM-1 residues (*Upper Insets* in Fig. 4 *A* and *B*). Despite these differences, the binding site and conformation are very close to the design model, demonstrating the power of the computational design methods used.

Peptide NDM1i-1F differs from NDM1i-1G by an I6V mutation, effectively replacing one methyl group by a hydrogen atom. This small change results in an approximately two-fold reduction in binding affinity. Differences in the crystal structures of NDM1i-1F and NDM1i-1G help to explain this. The C_δ atom in NDM1i-1G L-Ile6 is buried between Met67 and Phe70 on the HL hydrophobic face (Fig. 4*B*). When this atom is removed, Met67 adopts an alternative conformation allowing a small (0.7 Å) shift of the HL to fill the void (*SI Appendix*, Fig. S7). This rearrangement may account for the change in binding affinity. Like NDM1i-1G, peptide NDM1i-1F binds in a binding mode that resembles the design, with the HL shifting by 3.7 Å, and the peptide rotating in the opposite direction by 1.3 Å (backbone heavyatom rmsds). The backbone heavyatom rmsd between the superimposed peptide portion of the design model and the crystal structure is 0.4 Å, again indicating atomic-resolution accuracy in computational design of the peptide conformation itself.

Incorporation of Noncanonical Side Chains. Our attempts to design NDM-1 inhibitors were carried out concurrently with development work to enhance the computational methods to expand the set of noncanonical amino acid building blocks available for computational design (*SI Appendix*, section 1). Past design

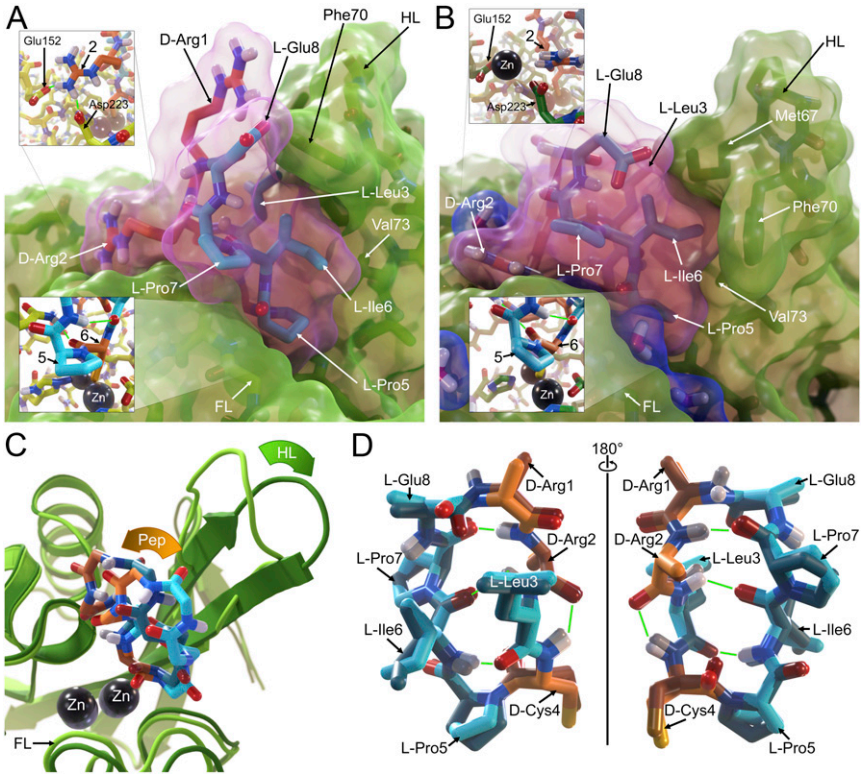

Fig. 4. Comparison of computational design model and X-ray crystal structure (PDB ID 6XBF) of peptide NDM1i-1G bound to NDM-1. In all panels, peptide L- and D-amino acid residues are shown as cyan and orange sticks, respectively. (*A*) Design model of NDM1i-1G (pink surface) in the active-site cleft of NDM-1 (green surface) with peptide residues L-Leu3 and L-Ile6 making contact with Met67 and Phe70 of the HL. The side chain of residue D-Arg1 was not resolved. (*Top Inset*) Peptide D-Arg2 projects toward the FL, making contact with Glu152 and Asp223. (*Lower Inset*) Stub residues L-Pro5 and D-Cys6 occlude the active site as L-captopril does, with D-Cys6 coordinating both active-site zinc atoms. (*B*) X-ray crystal structure of NDM1i-1G (pink surface) bound to NDM-1 (green surface). Crystallographic water molecules are shown as blue surfaces. Peptide residues L-Leu3 and L-Ile6 contact HL residues Met67 and Phe70, albeit in a slightly different configuration than designed. The D-Arg1 side chain was not resolved. (*Top Inset*) Glu-152 and Asp-223 coordinate a zinc cation, displacing the side chain of D-Arg2. (*Bottom Inset*) The L-Pro5, D-Cys6 stub occludes the active site as designed. (*C*) Overlay of design (lighter colors) and crystal structure (darker colors). The flexible HL undergoes a 3.1-Å shift (green arrow), while the peptide rotates slightly about its base, resulting in a 1.8 Å rmsd (orange arrow). (*D*) Overlay of peptide portion of design (lighter colors) aligned to peptide portion of crystal structure (darker colors). The peptide's internal conformation matches the design to a backbone heavyatom rmsd of 0.3 Å with side-chain rotamers of L-Leu3 and L-Ile6 closely aligning. All four designed internal hydrogen bonds (green lines) were present in the experimentally observed conformation.

efforts involving exotic noncanonical building blocks used an energy function inspired by molecular dynamics force fields (25), but in the context of a target protein, this would lose the advantages of the Rosetta energy function, which has been highly optimized to reproduce conformational preferences of proteinogenic amino acids. We therefore opted to use the Rosetta ref2015 energy function with computed side-chain potentials produced by the MakeRotLib application, as described in *SI Appendix*, sections 1.1 and 1.2. We explored whether an expanded palette of amino acid building blocks could unlock new inhibition mechanisms.

Using the crystal structure of NDM1i-1G as our starting point, we sampled perturbations of the bound conformation of this peptide and designed sequences incorporating several noncanonical side chains (*SI Appendix*, Table S1). We found that many design trajectories converged to include L-norleucine (L-Nlu) at position 3, 2-aminomethyl-L-phenylalanine (L-A34) at position 6, and (4R)-4-hydroxy-L-proline (L-Hyp) at position 7. We synthesized and tested four designs with predicted fold propensities above 0.9 that incorporated these noncanonical amino acids, shown in *SI Appendix*, Fig. S8. One of these, NDM1i-3D, had an IC_{50} value of 3.1 ± 0.3 μM, close to that of NDM1i-1G.

We solved the X-ray crystal structure of peptide NDM1i-3D bound to NDM-1 and found that, although this peptide did occlude the NDM-1 active site, its binding mode was inverted relative to the design, with residue L-Glu8, rather than D-Cys4, coordinating the active-site zinc atoms (Fig. 5). When the crystal structure and design model of the complex were aligned, the peptide backbone heavyatom rmsd was 9.4 Å due to this inversion. The HL conformation was closer to the design than in the cases of NDM1i-1F and -1G, deviating by a backbone heavyatom rmsd of 1.2 Å. Despite this, the peptide was rigidly structured in the designed conformation: superposition of the peptide portion of the structure yielded a backbone heavyatom rmsd of 0.4 Å from design to crystal structure.

A similar rotation by ∼180° was observed previously in the X-ray crystal structure of a two-sided de novo-designed heterodimer interface between two protein scaffolds (26). Although the peptide macrocycle designed here is very different from the protein scaffold in this previous study, both have in common a certain rough symmetry: both present side chains in a manner that is roughly preserved on 180° rotation. In the case of the designed protein, 180° rotation roughly preserves the location of repeated helices. In the case of the designed macrocycle, the peptide superimposes on its own four-residue cyclic permutation, corresponding to a 180° rotation, with a backbone heavyatom rmsd of 2.0 Å. This cyclic permutation places each of the hydrophobic L-Nlu and L-A34 side chains in the space that the other formerly occupied, while permitting L-Glu8 to replace D-Cys4 at the metal-binding position (Fig. 5*E*). Future design

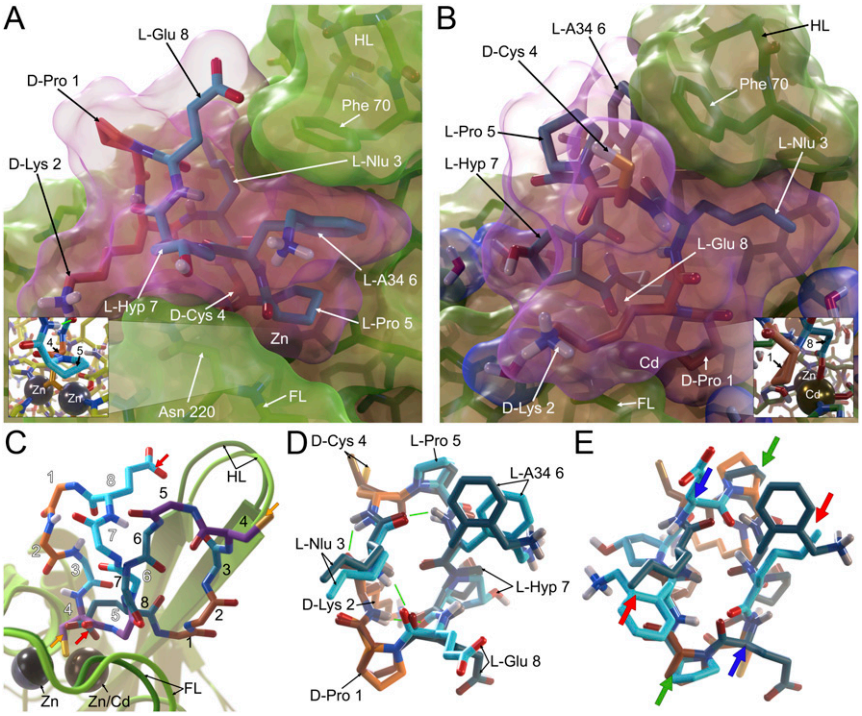

Fig. 5. Comparison of design model and crystal structure (PDB ID 6XCI) of peptide NDM1i-3D bound to NDM-1. (*A*) Design model of NDM1i-3D (pink surface, with L- and D-amino acid residues shown in cyan and orange, respectively) in the NDM-1 active site (green). L-2-aminomethyl phenylalanine (L-A34) and L-norleucine (L-Nlu) residues make hydrophobic contacts with the inner face of the HL. (*Inset*) D-Cys at position 5 coordinates active-site zinc atoms. (*B*) X-ray crystal structure of NDM1i-3D bound to NDM-1. The peptide is rotated nearly 180° relative to the design model with L-Nlu and L-A34 residues in opposite positions. Water molecules are shown as sticks with blue surfaces. (*Inset*) L-Glu at position 8 coordinates the active-site zinc. Cadmium is observed in place of zinc at the adjacent site. (*C*) Overlay of X-ray crystal structure (darker colors) and design model (lighter colors). NDM-1 is shown in green; L- and D-amino acids in NDM1i-3D are shown in cyan and orange, respectively, and stub residues are shown in purple. The crystal structure's positions are labeled in black, and the design model's positions in white. As shown, the rotation of the design model puts L-Glu-8 (red arrows) where D-Cys-4 (orange arrows) would be. The motion of the peptide displaces it by an rmsd of 9.4 Å, while the HL moves by 1.2 Å. (*D*) Overlay of aligned peptide portions of the crystal structure (darker colors) and design model (lighter colors). Cyan and orange represent L- and D-amino acids, as before. Despite the change in binding orientation, the crystal structure peptide conformation matches the design to a backbone heavyatom rmsd of 0.4 Å. (*E*) Overlay of crystal structure with peptide design circularly permuted by four residues. The rough symmetry of the backbone conformation allows D-Pro 1 to occupy the space that would be occupied by L-Pro 5 (green arrows), D-Cys 4 to occupy the space that would be occupied by L-Glu 8 blue arrows), and L-Nlu 3 to occupy the space that would be occupied by L-A34 6 (red arrows), possibly explaining why the peptide was able to bind to the same site in a very different binding mode.

efforts may be able to anticipate cases of correct localization but incorrect orientation by identifying scaffold symmetries that may give rise to roughly equivalent binding modes. In order to determine whether we could have detected the alternative mode had we sampled it, we relaxed and scored both the NDM1i-3D design model and the X-ray crystal structure using a protocol designed to preserve the cyclic geometry and metal coordination geometry (*SI Appendix*, section 2.1.7). The protocol captures the noncovalent interactions between macrocycle and target, but does not attempt to distinguish the binding energy of a cysteine side chain forming a bond to a zinc ion (as in the design model) vs. a glutamate side chain forming a bond to a cadmium ion (as in the crystal structure), which requires detailed quantum mechanics calculations. We found that Rosetta does indeed predict that the inverted binding mode seen in the crystal structure is lower in energy, with a computed energy of −356.74 kcal/mol, than the designed binding mode, which had a computed energy of −352.35 kcal/mol.

A final round of designs based on this alternative binding orientation and incorporating bulkier hydrophobic groups to try to maximize interactions with the hydrophobic face of the HL did not yield better inhibitors, likely due to poorer propensity to favor the binding-competent conformation (*SI Appendix*, Fig. S9 and section 4.3).

Conclusions

We have introduced general computational methods for designing peptide macrocycles to bind to targets of therapeutic interest. Unlike screening-based approaches, computational design allows the creation of molecules able to bind to a desired site and in a desired binding mode. Of our seven NDM1i-1 designs, six were stronger inhibitors than the D-captopril control (itself a stronger inhibitor than the L-captopril starting point for design). By explicitly considering the propensity of a peptide macrocycle to favor a binding-competent conformation, we were able to predict the rank order of IC_{50} values, supporting our working hypothesis that the entropic cost of ordering larger molecules on binding must be minimized, while also providing a useful tool for in silico screening of future designs. X-ray crystallography confirmed that our top binders, NDM1i-1F and NDM1i-1G, bound to the active site in a binding mode very close to that designed, with flexibility of a flanking loop accounting for deviation from the design.

Accurately predicting the effect of point mutations on binding in silico can be difficult, as observed in our characterization of peptides NDM1i-2A through 2K, making experimental screens of variants of computationally designed starting points a useful complement. The fact that peptide NDM1i-2J, found in a very small experimental screen of variants, has inhibitory activity comparable to the NDM1i-1G starting point despite differing in

sequence at three of eight positions suggests that scaffolds with high propensity to favor the binding-competent conformation provide good starting points for more extensive optimization of binding affinity through mutagenesis experiments.

Challenges for computational macrocycle design include the difficulty of considering the possible conformations of the peptide macrocycle backbone, the possible conformations of the loops flanking the target site, and the possible orientations of the peptide relative to the target. It can also be difficult to correctly model the conformational energetics of exotic chemical building blocks. Both of these may have contributed to the serendipitous discovery of an alternative binding mode of peptide NDM1i-3D, although the finding that this peptide adopted the designed backbone conformation raises the possibility of designing peptides with internal quasi-symmetry that have multiple possible binding modes for a target (27).

With the 29 peptides described here, including 6 with IC_{50} and K_I values under 5 μM (*SI Appendix*, Table S3), we demonstrate an approach for the rapid identification of hits to inhibit antibiotic resistance factors. That these molecules are highly mutable provides a means of producing variants to continue the "arms race" as resistance mechanisms evolve. More broadly, these techniques could offer an alternative to costly high-throughput compound library screens for a broad range of targets of therapeutic interest.

Materials and Methods

Enhancements of the Rosetta Software Suite. The computational work described here was carried out with the Rosetta software suite, a set of C++ libraries and applications for heteropolymer design, structure prediction, and modeling (11). Software enhancements needed to enable this work included improved support for energetic calculations involving noncanonical amino acids with the protein-centric ref2015 energy function (22, 23), the implementation of four new design-centric guidance scoring terms to control the design process, the creation of new tools for modeling metalloproteins, a new module for efficiently counting internal backbone hydrogen bonds in a peptide, support for automatic and massively parallel ensemble analysis during peptide structural validation, and other miscellaneous improvements to the kinematic machinery and design interface. These are described in full detail in *SI Appendix*, section 1, and are documented on the Rosetta help wiki (https://www.rosettacommons.org/docs/latest/Home). All enhancements to the software have been incorporated into public Rosetta releases. Rosetta is available from https://www.rosettacommons.org/. Compiled executables and source code are made freely available to academics, government users, and not-for-profit users and are licensed for for-profit use by way of a fee paid through University of Washington CoMotion (https://els2.comotion.uw.edu/product/rosetta).

Computational Protocols. NDM1i-1 peptides were designed by starting with the structure of NDM-1 bound to L-captopril (PDB ID 4EXS). L-captopril resembles a D-cysteine-L-proline dipeptide but for a methyl group that replaces the terminal amine. In silico, we converted L-captopril in the active-site pocket to a dipeptide and extended it with a polyglycine sequence to make an octapeptide, which we cyclized using Rosetta's generalized kinematic closure protocol. This approach is general and can be applied to starting stubs from experimentally solved complexes or from in silico docking. We discarded conformations with fewer than three internal backbone hydrogen bonds, those with oversaturated hydrogen bond acceptors, or those with egregious clashes between the macrocycle backbone and the target. We then used Rosetta's rotamer optimization module (the Rosetta packer) to design the peptide sequence while simultaneously sampling alternative packings of nearby side chains on the NDM-1 target. We refined the initial design through a Monte Carlo search in which moves consisted of small perturbations of the macrocycle backbone (maintaining closure using generalized kinematic closure) and side-chain reoptimization. Top conformations encountered during the Monte Carlo trajectory were more rigorously redesigned using the Rosetta FastDesign protocol (12). To select designs for synthesis, metrics such as shape complementarity and overall Rosetta energy were considered. We also sought diversity in the design pool using backbone bin strings to classify conformations, as described in *SI Appendix*, section 2.1.6. In addition, top peptides were subjected to conformational landscape analysis using the Rosetta simple_cycpep_predict application, which computed the P_{Near} metric and produced an estimate of the peptide $\Delta G_{folding}$. See *SI Appendix*, section 1.5.4, for details on both calculations, and *SI Appendix*, sections 2.1.1 and 2.2.2, for details on the design protocol.

NDM1i-2 designs were variants on NDM1i-1G. Four point mutants were selected using in silico mutational scanning and P_{Near} analysis (*SI Appendix*, Fig. S3). These, and seven combinations of these mutations, were synthesized and tested.

NDM1i-3 designs were designed using a variant of the protocol used to produce NDM1i-1 designs. Starting with the X-ray crystal structure of NDM1i-1G bound to NDM-1 (Fig. 4), the macrocycle was subjected to small perturbations and redesigned using a much-expanded palette of amino acid building blocks. The step of performing extensive macrocycle backbone conformational sampling via a Monte Carlo search was omitted. To be as conservative as possible, we constrained the number of exotic noncanonical amino acids to one to two per design using the aa_compostion design-centric guidance scoring term (13). We also made use of newly developed design-centric terms (described in *SI Appendix*, section 1.3) to encourage desired properties during design. See *SI Appendix*, sections 2.1.2 and 2.2.3, for details on the design protocol, and *SI Appendix*, Table S1, for the exotic amino acid types considered during the design process.

Based on the alternative conformation observed in the X-ray crystal structure of NDM1i-3D bound to NDM-1, (Fig. 5), we redesigned the macrocycle using a more broadly expanded palette of amino acid building blocks (*SI Appendix*, Table S1) to produce the NDM1i-4 designs. We also altered the protocol used for NDM1i-3 designs by adding sampling of small perturbation of the HL in addition to the macrocycle backbone, relaxing the restrictions on the number of exotic side chains that could be incorporated and including crystallographic water molecules during design as hydrogen bond donors and acceptors. See *SI Appendix*, section 2.1.3, for the full design protocol.

All computational protocols are provided as RosettaScripts XML scripts (28) in *SI Appendix*, section 2, along with all supporting files and information needed to reproduce the design protocol. These scripts and supporting files are also available from GitHub (https://github.com/vmullig/ndm1_design_scripts) (29), and from the RosettaCommons RosettaScripts scripts repository.

Enzymatic Assays and Data Analysis. NDM-1 was expressed in and purified from *Escherichia coli* BL21(DE3) cells. Inhibition of the hydrolysis of 1.5 μM nitrocefin was assayed as described in *SI Appendix*, section 3.3. D-Captopril was used as a positive control (*SI Appendix*, Fig. S1). NDM-1 activity was plotted as a function of inhibitor concentration, and data were fitted with SciPy using a modified Hill equation to extract IC_{50} values, as described in *SI Appendix*, section 3.3. Since all inhibition assays were performed with a constant initial concentration of substrate, IC_{50} values were proportional to K_I values, allowing direct comparison across inhibitors; however, K_I values for all peptides are also reported in *SI Appendix*, section 4.1.

X-Ray Crystallography. For crystallization, NDM-1 was expressed in and purified from *E. coli* BL21(DE3) cells as described in *SI Appendix*, section 3.4.1. NDM1i-1F, NDM1i-1G, or NDM1i-3D peptide was added to the protein, and crystals were grown by the hanging-drop method; full details are provided in *SI Appendix*, section 3.4.2. Following cryoprotection with 25% glycerol and immersion in liquid nitrogen, diffraction data for NDM1i-1F and NDM1i-1G were collected on beamline 08ID-1 at the Canadian Light Source, at 100 K using a wavelength of 0.979 Å. Data for NDM1i-3D were collected on beamline 5.0.1 at the Advanced Light Source, at 100 K using a wavelength of 0.977 Å. The structure of NDM-1 with no peptide bound (PDB ID 3SPU) was used for molecular replacement phasing. Model validation was carried out with MoLProbity (30) with the NDM1i-1F complex having 99.02 and 0.22%, the NDM1i-1G complex having 98.69 and 0%, and NDM1i-3D having 98.88 and 0% Ramachandran-favored and outliers, respectively. Full details of analysis and refinement are provided in *SI Appendix*, section 3.4.2, and data processing, refinement, and model statistics are shown in *SI Appendix*, Table S3.

Data Availability. RosettaScripts XML scripts for peptide macrocycle inhibitor design data have been deposited in GitHub (https://github.com/vmullig/ndm1_design_scripts), and are also available in the *SI Appendix*. Structure factors and coordinates for the NDM1i-1F, NDM1i-1G, and NDM1i-3D complexes have been deposited in the Protein Data Bank (PDB IDs 6XBE, 6XBF, and 6XCI, respectively).

ACKNOWLEDGMENTS. V.K.M., P.D.R., and R.B. were supported by the Simons Foundation. S.W. was supported by an Alexander Graham Bell Canada Graduate Scholarship from the Natural Sciences and Engineering Research Council. T.S. was supported by a Michael Smith Foundation for

Health Research Postdoctoral Fellowship. D.T.K. was supported by a doctoral award from the Canadian Institutes of Health Research (CIHR). P.H. and T.W.C. were supported by Washington Research Foundation Innovation postdoctoral fellowships. P.H. was also supported by NIH Ruth Kirschstein F32 award no. F32GM120791-02. A.M.W. was supported by NIH Grant R21 CA219847. J.W.L. was supported by the NIH Grants 1F32-CA189246 and R01-GM127578 and by the RosettaCommons. R.M. was supported by the RosettaCommons. N.C.J.S. was supported by operating funds awarded from the CIHR and Tier 1 Canada Research Chair program. D.B. was supported by the Howard Hughes Medical Institute. Crystallographic data were collected using beamline 08ID-1 at the Canadian Light Source, which is supported by the Canada Foundation for Innovation, Natural Sciences and Engineering Research Council of Canada, the University of Saskatchewan, the Government of Saskatchewan, Western Economic Diversification Canada, the National Research Council Canada, and the CIHR. Crystallographic data were also accrued at the Advanced Light Source, a Department of Energy (DOE) Office of Science User Facility under contract no. DE-AC02-05CH11231. The authors thank the staff of beamline 5.0.2 for their assistance and Fred Rosell for advice on the nitrocefin assay. An award of computer time was provided to D.B. and V.K.M. by the Innovative and Novel Computational Impact on Theory and Experiment program. This research used resources of the Argonne Leadership Computing Facility, which is a DOE Office of Science User Facility supported under Contract DE-AC02-06CH11357. Computations were carried out on the Mira and Theta supercomputers at Argonne National Laboratory, the University of Washington Hyak cluster, and the Simons Foundation Iron, Gordon, and Popeye clusters. We thank Andrew Leaver-Fay and Sergey Lyskov for Rosetta support and Yuri Alexeev for support on Mira and Theta.

1. R. J. Worthington, C. Melander, Overcoming resistance to β-lactam antibiotics. *J. Org. Chem.* **78**, 4207–4213 (2013).
2. K. E. Rudd *et al*., Global, regional, and national sepsis incidence and mortality, 1990–2017: Analysis for the global burden of disease study. *Lancet* **395**, 200–211 (2020).
3. K. Bush, Proliferation and significance of clinically relevant β-lactamases. *Ann. N. Y. Acad. Sci.* **1277**, 84–90 (2013).
4. D. Yong *et al*., Characterization of a new metallo-β-lactamase gene, bla(NDM-1), and a novel erythromycin esterase gene carried on a unique genetic structure in Klebsiella pneumoniae sequence type 14 from India. *Antimicrob. Agents Chemother.* **53**, 5046–5054 (2009).
5. K. K. Kumarasamy *et al*., Emergence of a new antibiotic resistance mechanism in India, Pakistan, and the UK: A molecular, biological, and epidemiological study. *Lancet Infect. Dis.* **10**, 597–602 (2010).
6. Centers for Disease Control and Prevention (CDC), Detection of Enterobacteriaceae isolates carrying metallo-beta-lactamase: United States, 2010. *MMWR Morb. Mortal. Wkly. Rep.* **59**, 750 (2010).
7. P. Deshpande *et al*., New Delhi metallo-beta lactamase (NDM-1) in Enterobacteriaceae: Treatment options with carbapenems compromised. *J. Assoc. Physicians India* **58**, 147–149 (2010).
8. A. M. Somboro, J. Osei Sekyere, D. G. Amoako, S. Y. Essack, L. A. Bester, Diversity and proliferation of metallo-β-lactamases: A clarion call for clinically effective metallo-β-lactamase inhibitors. *Appl. Environ. Microbiol.* **84**, e00698-18 (2018).
9. J. W. Scannell, A. Blanckley, H. Boldon, B. Warrington, Diagnosing the decline in pharmaceutical R&D efficiency. *Nat. Rev. Drug Discov.* **11**, 191–200 (2012).
10. M. H. Baig *et al*., Computer aided drug design: Success and limitations. *Curr. Pharm. Des.* **22**, 572–581 (2016).
11. A. Leaver-Fay *et al*., "Rosetta3" in *Methods in Enzymology*, M. L. Johnson, L. Brand, Eds. (Elsevier, 2011), pp. 545–574.
12. G. Bhardwaj *et al*., Accurate de novo design of hyperstable constrained peptides. *Nature* **538**, 329–335 (2016).
13. P. Hosseinzadeh *et al*., Comprehensive computational design of ordered peptide macrocycles. *Science* **358**, 1461–1466 (2017).
14. B. Dang *et al*., De novo design of covalently constrained mesosize protein scaffolds with unique tertiary structures. *Proc. Natl. Acad. Sci. U.S.A.* **114**, 10852–10857 (2017).
15. V. K. Mulligan, The emerging role of computational design in peptide macrocycle drug discovery. *Expert Opin. Drug Discov.* **15**, 833–852 (2020).
16. J. A. DiMasi, L. Feldman, A. Seckler, A. Wilson, Trends in risks associated with new drug development: Success rates for investigational drugs. *Clin. Pharmacol. Ther.* **87**, 272–277 (2010).
17. H. M. Dintzis, D. E. Symer, R. Z. Dintzis, L. E. Zawadzke, J. M. Berg, A comparison of the immunogenicity of a pair of enantiomeric proteins. *Proteins* **16**, 306–308 (1993).
18. C. K. Wang, D. J. Craik, Cyclic peptide oral bioavailability: Lessons from the past. *Biopolymers* **106**, 901–909 (2016).
19. D. King, N. Strynadka, Crystal structure of New Delhi metallo-β-lactamase reveals molecular basis for antibiotic resistance. *Protein Sci.* **20**, 1484–1491 (2011).
20. D. T. King, L. J. Worrall, R. Gruninger, N. C. J. Strynadka, New Delhi metallo-β-lactamase: Structural insights into β-lactam recognition and inhibition. *J. Am. Chem. Soc.* **134**, 11362–11365 (2012).
21. Y. Guo *et al*., A structural view of the antibiotic degradation enzyme NDM-1 from a superbug. *Protein Cell* **2**, 384–394 (2011).
22. R. F. Alford *et al*., The rosetta all-atom energy function for macromolecular modeling and design. *J. Chem. Theory Comput.* **13**, 3031–3048 (2017).
23. H. Park *et al*., Simultaneous optimization of biomolecular energy functions on features from small molecules and macromolecules. *J. Chem. Theory Comput.* **12**, 6201–6212 (2016).
24. S. J. Fleishman, D. Baker, Role of the biomolecular energy gap in protein design, structure, and evolution. *Cell* **149**, 262–273 (2012).
25. P. D. Renfrew, E. J. Choi, R. Bonneau, B. Kuhlman, Incorporation of noncanonical amino acids into Rosetta and use in computational protein-peptide interface design. *PLoS One* **7**, e32637 (2012).
26. J. Karanicolas *et al*., A de novo protein binding pair by computational design and directed evolution. *Mol. Cell* **42**, 250–260 (2011).
27. V. K. Mulligan *et al*., Computational design of mixed chirality peptide macrocycles with internal symmetry. *Protein Sci.* **29**, 2433–2445 (2020).
28. S. J. Fleishman *et al*., RosettaScripts: A scripting language interface to the Rosetta macromolecular modeling suite. *PLoS One* **6**, e20161 (2011).
29. V. K. Mulligan, Scripts for NDM-1 peptide macrocycle inhibitor design and analysis. Github. https://github.com/vmullig/ndm1_design_scripts. Deposited 8 December 2020.
30. C. J. Williams *et al*., MolProbity: More and better reference data for improved all-atom structure validation. *Protein Sci.* **27**, 293–315 (2018).